Anisotropy of acoustooptic figure of merit for TeO_2 crystals. 1. Isotropic diffraction

Mys O., Kostyrko M., Smyk M., Krupych O. and Vlokh R.

Vlokh Institute of Physical Optics, 23 Dragomanov Str., 79005 Lviv, Ukraine, vlokh@ifo.lviv.ua

Received: 23.05.2014

Abstract. present the method for analyzing the anisotropy of acoustooptic figure of merit for optically uniaxial crystals and illustrate it on the example of crystalline paratellurite. This first part of the article deals with analysis of the isotropic acoustooptic interaction. The results of our calculations agree well with the experimental data known from the literature.

Keywords: acoustooptic figure of merit, effective elastooptic coefficients, paratellurite crystals, anisotropy

PACS: 43.35.Sx, 42.70.Mp
UDC: 535.012.2+535.42+534.321.9

1. Introduction

Crystalline tellurium dioxide or paratellurite, TeO_2, is optically uniaxial and positive, and belongs to tetragonal point symmetry group 422 [1]. It is characterized by high enough refractive indices ($n_o = 2.2597$ and $n_e = 2.4119$ at the light wavelength of $\lambda = 632.8$ nm [2]). TeO_2 crystal reveals a noticeable optical activity effect: its rotatory power is as large as (86.9±0.5) deg/mm at 632.8 nm [2]. Perhaps, the most important property of paratellurite is high acoustooptic (AO) efficiency. Therefore TeO_2 is one of the renown crystalline AO materials, being among such substances as mercurous halides (Hg_2Cl_2 and Hg_2Br_2) [3, 4] or chalcogenides (e.g., Tl_3PSe_4 [5]).

Earlier we have shown [6] that the AO prominence of paratellurite appears owing to ferroelasticity of this crystal. It exhibits a ferroelastic tetragonal-to-orthorhombic phase transition under high pressures [7]. The transition is accompanied by softening of the acoustic phonon which propagates along the direction [110] and is polarized parallel to $[1\bar{1}0]$ [8]. As a matter of fact, the maximum AO figure of merit (AOFM) M_2 at the normal conditions, which is equal to 1200×10^{-15} s^3/kg [9], is just achieved in the case of anisotropic AO interaction with the acoustic wave (AW) described above. Notice also that the highest AOFM in TeO_2 crystals is observed when the light eigenwaves are almost circularly polarized. In other words, then the incident circularly polarized light propagates along the direction close to the optic axis where the natural optical activity affects essentially the eigenwave polarization [9]. When the incident optical wave of different polarizations interacts with the slowest AW, the AOFM of TeO_2 crystals is also very high. For example, the AOFM is decreased only down to $(600-800)\times10^{-15}$ s^3/kg [9] for the AO interaction of arbitrarily (or linearly) polarized incident waves with the same shear AW.

Probably, the most comprehensive experimental data for the AOFM of TeO_2 crystals are presented in Ref. [10] (These data are collected for a comparison in Table 1 appearing in the final chapter of this work). However, all of those values have been reported only for the cases when the

propagation and polarization directions of the optical wave and the AW are parallel to the principal crystallographic directions. At the same time, one cannot exclude that still larger M_2 values can exist, which correspond to the interaction of waves propagating along arbitrary directions with respect to the crystallographic coordinate system. Let us consider this point in detail. The AOFM is given by the relation

$$M_2 = \frac{n^6 p_{ef}^2}{\rho v_{ij}^3}, \tag{1}$$

where ρ is the density of material, n its refractive index, v_{ij} the AW velocity (with the indices i and j corresponding to the AW propagation and polarization directions, respectively), and p_{ef} the effective elastooptic coefficient (EEC). The main contribution to the AOFM comes from the AW velocity and the EEC. In principle, certain values of these parameters can provide an interaction geometry for which the highest M_2 value is reached. In particular, the highest AOFM values are known to be reached for the cases of interactions with the slowest AW.

On the other hand, the slowness of the AW makes a negative influence on the switching speed of AO devices. This means that searching for experimental geometries in which the AOFM is high enough due to high EEC but not a slowness of the AW represents an important problem. This analysis still expects developing of the appropriate techniques. Recently we have suggested an analytical approach for analyzing the spatial anisotropy of AOFM for the isotropic media and cubic crystals [11]. It has been shown that six different types of AO interactions are peculiar for the cubic crystals, each of these types being characterized by its own AOFM and revealing a certain anisotropy. Obviously, a number of the interaction types should increase for anisotropic optically uniaxial crystals, at least because the anisotropic types of AO diffraction should be involved into consideration.

The aim of the present work is to analyze the anisotropy of AOFM for TeO_2 crystals. This is based on a general analytical approach developed for assessing the spatial anisotropy of the M_2 parameter in the optically uniaxial crystals of point symmetry groups 4/mmm, 422, $\bar{4}$2m and 4mm. These point groups are characterized by the same tensors of elastic stiffness and elastooptic coefficients. In this first part of the study we present the analysis for the cases of isotropic AO diffraction.

2. Results of analysis

For the crystals of the point symmetries 4/mmm, 422, $\bar{4}$2m and 4mm, including the case of TeO_2, the elastic stiffness tensor contains six independent components (Voigt notation is used) $C_{11} = C_{22}$, C_{12}, $C_{13} = C_{23}$, C_{33}, $C_{44} = C_{55}$ and $C_{66} \neq (C_{11} - C_{12})/2$, while the elastooptic tensor has seven independent coefficients ($p_{11} = p_{22}$, $p_{12} = p_{21}$, $p_{13} = p_{23}$, $p_{31} = p_{32}$, p_{33}, $p_{44} = p_{55}$ and $p_{66} \neq (p_{11} - p_{12})/2$ [1]). When studying the anisotropy of M_2 coefficient for TeO_2 crystals, we will use the methods developed in our recent work [11]. Namely, we will construct and analyze cross sections of the surfaces of EEC, AW slowness and AOFM, which are obtained by rotating the interaction plane around Z and X axes that correspond to crystallographic axes c and a, respectively. Notice that, for all of the point groups 4/mmm, 422, $\bar{4}$2m and 4mm, the coordinate system XYZ is associated with eigenvectors of the optical Fresnel ellipsoid, being coincident with the crystallographic system abc.

To begin, let us consider the AW propagating in the *XZ* plane in TeO_2. The dependences of quasi-transverse AW velocities on the wave vector orientation in the *XZ* plane are as follows:

$$v_{QT_1}^2(\Theta) = \frac{(C_{11}+C_{44})\cos^2\Theta + \sin^2\Theta(C_{44}+C_{33})}{2\rho} - \\ - \frac{\sqrt{[(C_{11}-C_{44})\cos^2\Theta + (C_{44}-C_{33})\sin^2\Theta]^2 + 4\cos^2\Theta\sin^2\Theta(C_{13}+C_{44})^2}}{2\rho}, \quad (2)$$

$$v_{QT_2}^2(\Theta) = \frac{C_{44}\cos^2\Theta + C_{66}\sin^2\Theta}{\rho}. \quad (3)$$

The same relation for the quasi-longitudinal AW velocity takes the form

$$v_{QL}^2(\Theta) = \frac{(C_{11}+C_{44})\cos^2\Theta + \sin^2\Theta(C_{44}+C_{33})}{2\rho} + \\ + \frac{\sqrt{[(C_{11}-C_{44})\cos^2\Theta + (C_{44}-C_{33})\sin^2\Theta]^2 + 4\cos^2\Theta\sin^2\Theta(C_{13}+C_{44})^2}}{2\rho}, \quad (4)$$

where Θ is the angle between the AW vector and the *X* axis in the *XZ* plane, i.e. the angle of rotation of the AW vector around the *Y* axis (see Fig. 1a). For the other interaction planes rotated by some angles φ_Z around the *Z* axis (i.e., in the new coordinate systems $X'Y'Z$), the structure of the elastic stiffness tensor change, too. The new components of this tensor can be determined after rewriting this tensor in the new coordinate system according to a known procedure [1]. Performing this procedure for the elastic stiffness tensor, one can see that the components C'_{13}, $C'_{23} = C'_{13}$, C'_{33}, C'_{44} and $C_{55} = C_{44}$ remain the same, whereas the dependences of the coefficients $C'_{11}(\varphi_Z)$, $C'_{22}(\varphi_Z) = C'_{11}(\varphi_Z)$, $C'_{12}(\varphi_Z)$ and $C'_{66}(\varphi_Z)$ on the angle φ_Z are described as

$$\left.\begin{aligned} C'_{11}(\varphi_Z) &= C_{11} - \frac{1}{2}(C_{11}-C_{12}-2C_{66})\sin^2 2\varphi_Z \\ C'_{12}(\varphi_Z) &= C_{12} + \frac{1}{2}(C_{11}-C_{12}-2C_{66})\sin^2 2\varphi_Z \\ C'_{66}(\varphi_Z) &= C_{66} + \frac{1}{2}(C_{11}-C_{12}-2C_{66})\sin^2 2\varphi_Z \\ C'_{16}(\varphi_Z) &= -\frac{1}{4}(C_{11}-C_{12}-2C_{66})\sin 4\varphi_Z \end{aligned}\right\}. \quad (5)$$

The new elastic stiffness coefficients C'_{16} and C'_{26} appear in the tensor thus rewritten.

One can notice that the expressions for the components of the Christoffel tensor for each of the $X'Z$ planes remain the same as for the initial *XZ* plane. Substituting Eq. (5) into Eqs. (2)–(4), one obtains the AW velocities for all of the possible AW vector directions. As seen from Eq. (5), the presence of four-fold axis among the symmetry operations causes both the optical and acoustic equivalences of *a* and *b* directions and, as a result, the crystallographic planes *ac* and *bc* are also equivalent [1].

Rotation of the interaction plane by the angle φ_X around the *X* axis (see Fig. 1b) will change the expressions for the components of the Christoffel tensor and the elastic stiffness coefficients C'_{13}, C'_{33} and C'_{44}. The Christoffel tensor will become much more complicated. Then the AW velocities can be obtained using standard numeric techniques.

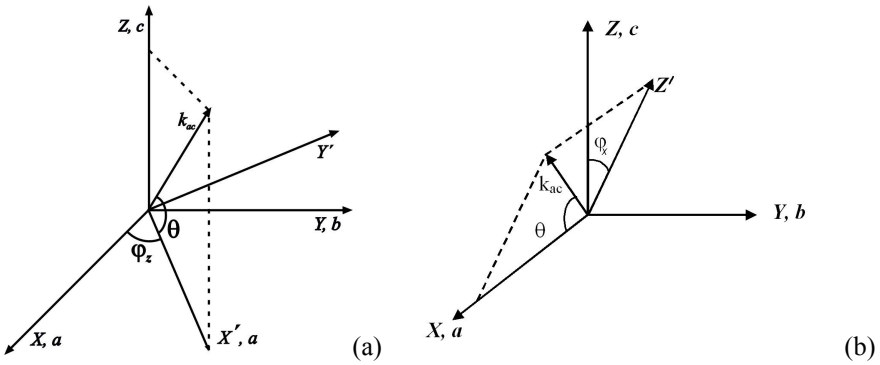

Fig. 1. Crystallographic coordinate system coupled with a Cartesian system *XYZ*, and a new coordinate system $X'Y'Z$ coupled with the plane $X'Z$ of AO interaction, as obtained under rotation of the interaction plane around *Z* (a) and *X* (b) axes.

Anisotropy of the acoustic and elastooptic properties of TeO_2 crystals allows a variety of possible types of AO interactions. Actually, we will demonstrate that there are nine different types of AO interactions in TeO_2 crystals. They include six types of isotropic interactions and three types of anisotropic interactions between the AWs and the optical waves. Regarding the isotropic interactions, one has the following interaction types.

Type (I): the AO interaction of the longitudinal AW propagating in the ZX' or $Z'X$ planes, and the incident optical wave with polarization of ordinary beam which is perpendicular to the interaction plane;

Type (II): the AO interaction of the longitudinal AW propagating in the ZX' or $Z'X$ planes, and the incident optical wave, with polarization of extraordinary beam, electric induction vector of which lies in the interaction plane at the angle θ_B with respect to the X or X' axis ($D_3 = D\sin\theta_B$ and $D_1 = D\cos\theta_B$, with D denoting the electric induction and θ_B the Bragg angle);

Type (III): the AO interaction of the transverse AW QT_1 propagating in the ZX' or $Z'X$ planes and polarized in the same planes, and the incident optical wave, with polarization of extraordinary beam, of which polarization vector lies in the interaction plane at the angle θ_B with respect to the X or X' axis ($D_3 = D\sin\theta_B$ and $D_1 = D\cos\theta_B$);

Type (IV): the AO interaction of the transverse AW QT_1 and the incident optical wave with polarization of ordinary beam which is perpendicular to the interaction plane;

Type (V): the AO interaction of the transverse AW QT_2 propagating along the X (X') axis and polarized along the Y (Y') axis, and the incident optical wave, with polarization of extraordinary beam, of which polarization vector lies in the interaction plane at the angle θ_B with respect to the X or X' axis ($D_3 = D\sin\theta_B$ and $D_1 = D\cos\theta_B$);

Type (VI): the AO interaction of the AW QT_2 and the incident optical wave with polarization of ordinary beam which is perpendicular to the interaction plane.

Since TeO_2 reveals large natural birefringence, the anisotropic types of interaction can be easily implemented in this material. There are three AO interaction types of the incident optical wave with the longitudinal AW and the two normal transverse AWs in TeO_2. These types of interaction will be considered in detail in the second part of this work.

When the AW induces changes in the extraordinary refractive index n_e due to elastooptic effect, the wave vector diagram will change for every new propagation direction of the AW in the

interaction planes (see Fig. 2a). Namely, this will change the Bragg angle, the lengths of the wave vectors of the incident and diffracted light waves, and the AW vector. The angle of orientation of the AW vector will change, too. These changes will impose changes in the induced elastic strain tensor components and, as a consequence, they will affect the EEC value. However, if we fix the Bragg angle, the angle Θ of inclination of the AW vector may be found using the relation between the tangential angle ψ and the polar angle ξ (see Fig. 3):

$$\cot\psi = -\frac{a^2 \tan\xi}{b^2}, \quad \Theta = \psi - 180, \tag{6}$$

where *a* and *b* stand for the semi axes of the Fresnel ellipsoid. Notice that for the known optically uniaxial crystalline materials, the deviations of the angle Θ from the value corresponding to the isotropic materials is small enough, since the elliptical cross section of the Fresnel ellipsoid surface is very close to a circle.

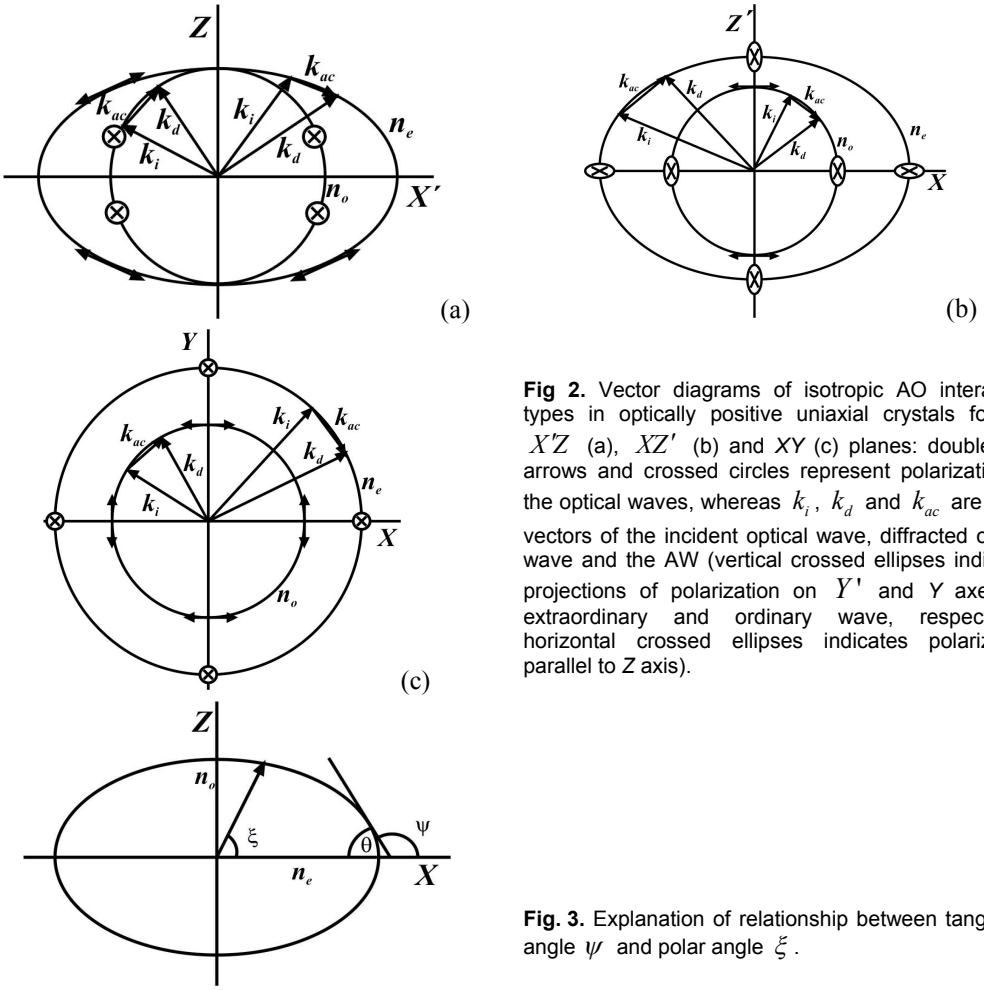

Fig 2. Vector diagrams of isotropic AO interaction types in optically positive uniaxial crystals for the $X'Z$ (a), XZ' (b) and *XY* (c) planes: double-side arrows and crossed circles represent polarization of the optical waves, whereas k_i, k_d and k_{ac} are wave vectors of the incident optical wave, diffracted optical wave and the AW (vertical crossed ellipses indicates projections of polarization on Y' and *Y* axes for extraordinary and ordinary wave, respectively; horizontal crossed ellipses indicates polarization parallel to *Z* axis).

Fig. 3. Explanation of relationship between tangential angle ψ and polar angle ξ.

Let us now consider in much detail the AO interaction type (I) when the quasi-longitudinal AW $v_{11} = v_{QL}$ propagating in the *XZ* plane interacts with the incident optical wave with the electric induction vector parallel to the *Y* axis. Suppose first that the longitudinal AW $v_{11} = v_{QL}$ propagates along the *X* direction. Then the electric field of the diffracted optical wave and the acoustically induced increment of the refractive index are as follows:

$$E_2 = \Delta B_2 D_2 = p_{21} e_1 D_2 , \tag{7}$$

$$\Delta n_2 = \frac{1}{2} n_o^3 p_{21} e_1 . \tag{8}$$

Rotation of the AW vector in the XZ plane means that we are to rewrite the strain tensor including the only component e_1 in the coordinate system rotated around the Y axis by the angle Θ. Then the three tensor components appear:

$$e'_1 = e_1 \cos^2 \Theta, \quad e'_3 = e_1 \sin^2 \Theta, \quad e'_5 = e_1 \sin \Theta \cos \Theta . \tag{9}$$

As a result, the EEC is given by.

$$p_{ef}^{(\mathrm{I})} = p_{21} \cos^2 \Theta + p_{23} \sin^2 \Theta, \quad (p_{21} = p_{12}, p_{23} = p_{13}) . \tag{10}$$

Under rotation of the interaction plane around the Z axis by the angle φ_Z, the deformation tensor components and the EEC will change to $e''_1 = e'_1 \cos^2 \varphi_Z$, $e''_2 = e'_1 \sin^2 \varphi_Z$, $e''_3 = e'_3$, $e''_4 = -e'_5 \sin \varphi_Z$, $e''_5 = e'_5 \cos \varphi_Z$, $e''_6 = -0.5 e'_1 \sin \varphi_Z \cos \varphi_Z$ and

$$\begin{aligned} p_{ef}^{(\mathrm{I})} = {} & \sin^2 \varphi_Z \left(p_{11} \cos^2 \Theta \cos^2 \varphi_Z + p_{12} \cos^2 \Theta \sin^2 \varphi_Z + p_{13} \sin^2 \Theta \right) \\ & + \cos^2 \varphi_Z \left(p_{21} \cos^2 \Theta \cos^2 \varphi_Z + p_{22} \cos^2 \Theta \sin^2 \varphi_Z + p_{23} \sin^2 \Theta \right) . \\ & + p_{66} \sin^2 2\varphi_Z \cos^2 \Theta \end{aligned} \tag{11}$$

Under rotation of the interaction plane around the X axis by the angle φ_X, the deformation tensor components and the EEC may be written as, $e'''_1 = e'_1$, $e'''_2 = e'_3 \sin^2 \varphi_X$, $e'''_3 = e'_3 \cos^2 \varphi_X$, $e'''_4 = -0.5 e'_3 \sin \varphi_X \cos \varphi_X$, $e'''_5 = e'_5 \cos \varphi_X$, $e'''_6 = -e'_5 \sin \varphi_X$ and

$$\begin{aligned} p_{ef}^{(\mathrm{I})} = {} & \left[\frac{\sin \varphi_X \cot(\Theta + \theta_b)}{\sqrt{1 + \sin^2 \varphi_X \cot^2 (\Theta + \theta_b)}} \right]^2 \\ & \times \left(p_{11} \cos^2 \Theta + p_{12} \sin^2 \Theta \sin^2 \varphi_X + p_{13} \sin^2 \Theta \cos^2 \varphi_X \right) + \\ & + \left[\frac{1}{\sqrt{1 + \sin^2 \varphi_X \cot^2 (\Theta + \theta_b)}} \right]^2 \\ & \times \left(p_{21} \cos^2 \Theta + p_{22} \sin^2 \Theta \sin^2 \varphi_X + p_{23} \sin^2 \Theta \cos^2 \varphi_X \right) + \\ & + 2 p_{66} \left[\frac{2 \sin \varphi_X \cot(\Theta + \theta_b)}{1 + \sin^2 \varphi_X \cot^2 (\Theta + \theta_b)} \right]^2 \cos^2 \Theta \end{aligned} . \tag{12}$$

Then the AOFM for the type (I) of AO interaction becomes as follows:

$$M_2^{(\mathrm{I})} = \frac{n^6 \left\{ p_{ef}^{(\mathrm{I})} \right\}^2}{\rho \left[v_{QL}(\Theta, \varphi_{Z,X}) \right]^3} , \tag{13}$$

were $v_{QL}(\Theta, \varphi_{Z,X})$ defines the change in the AW velocity occurring in the $X'Z$ or XZ' planes.

As seen from Fig. 4 and Fig. 5, the anisotropy of the AOFM arises from the anisotropy of EEC. The parameter $M_2^{(\mathrm{I})}$ reaches its maximum 33.3×10^{-15} s^3/kg at Θ=90 deg and $\varphi_Z = 0$ and 180 deg, i.e. for the directions of AW propagation where the EEC $p_{ef}^{(\mathrm{I})}$ approach maximal value.

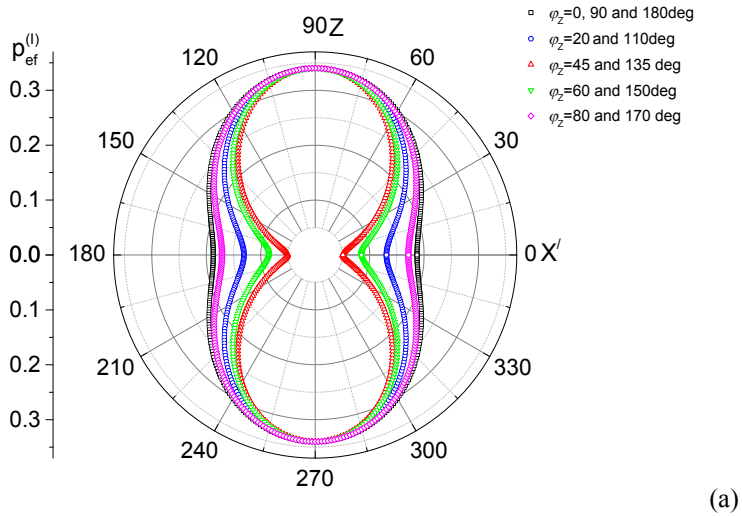

(a)

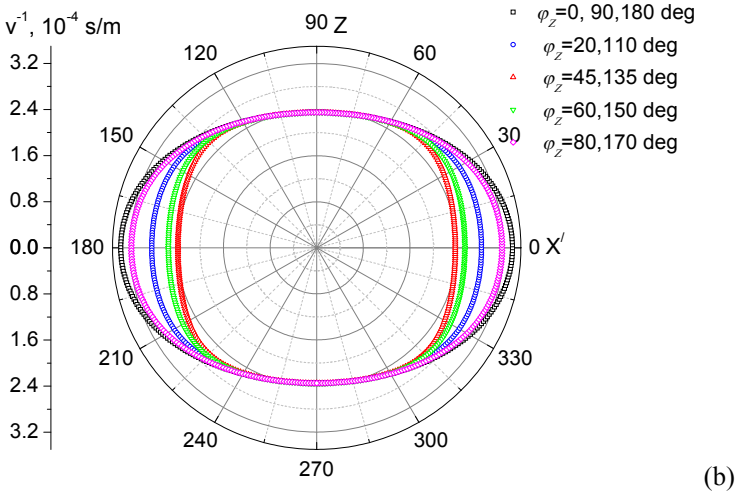

(b)

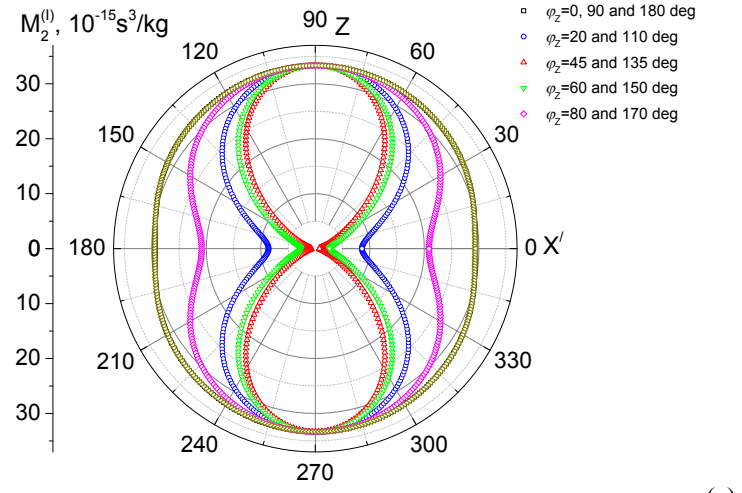

(c)

Fig. 4. Dependences of EEC $p_{ef}^{(I)}$ (a), AW slowness (b) and AOFM $M_2^{(I)}$ (c) on the direction of AW vector (angle Θ) at different orientations of the interaction plane (φ_Z is angle of rotation around the *Z* axis).

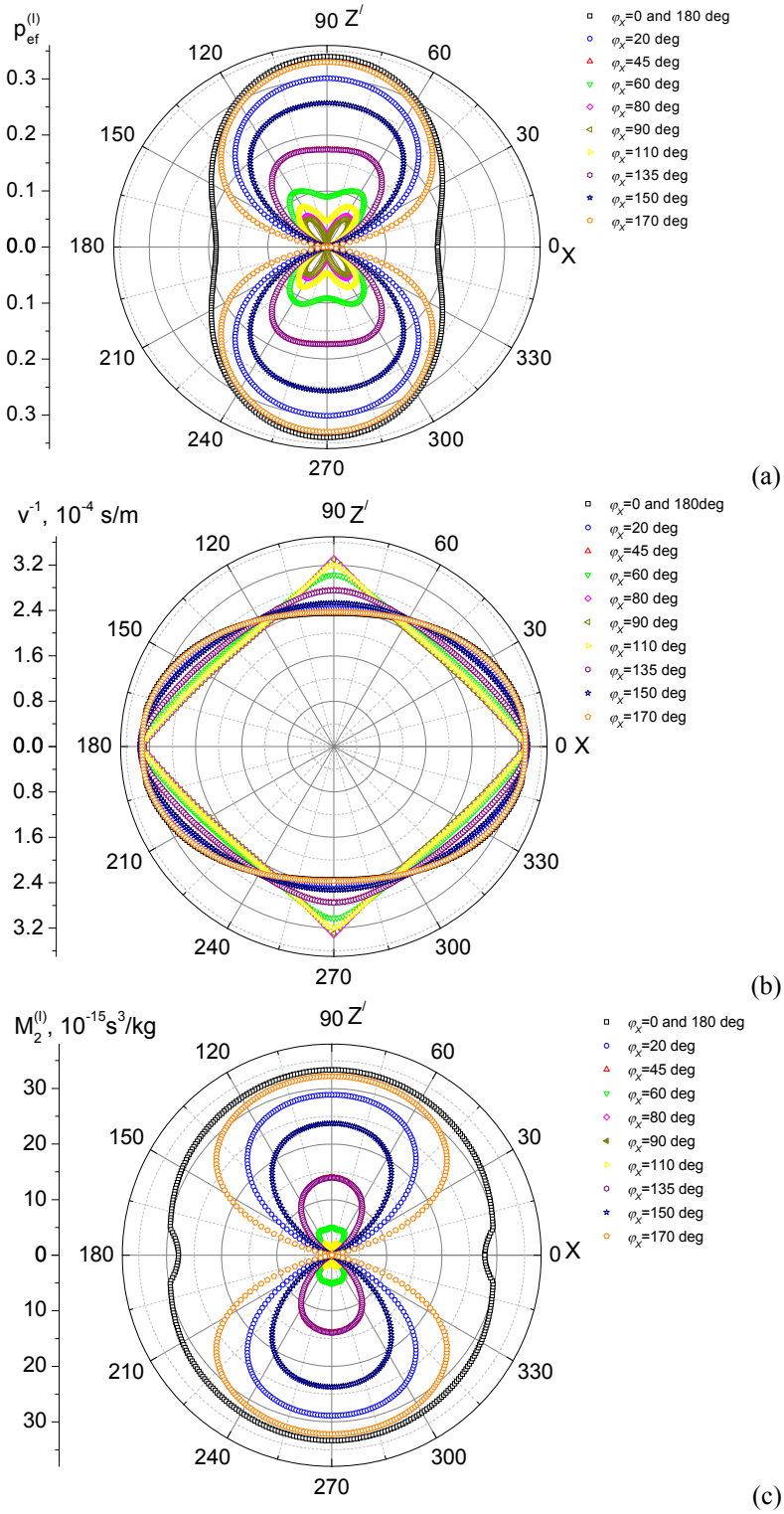

Fig. 5. Dependences of EEC $p_{ef}^{(I)}$ (a), AW slowness (b) and AOFM $M_2^{(I)}$ (c) on the direction of AW vector (angle Θ) at different orientations of the interaction plane (φ_X is angle of rotation around the *X* axis).

Let us proceed to the type (II) of AO interactions, when the longitudinal AW $v_{11} = v_{QL}$ propagating along the *X* axis interacts with the optical wave, of which electric induction vector lies in the *XZ* plane at the angle θ_B with respect to the *X* axis ($D_3 = D\sin\theta_B$ and $D_1 = D\cos\theta_B$). Here θ_B is chosen to be equal to 4 deg (see Ref. [11]). The electric field of the diffracted optical wave is given by

$$\begin{cases} E_1 = \Delta B_1 D_1 = p_{11} e_1 D_1 \\ E_3 = \Delta B_3 D_3 = p_{33} e_1 D_3 \end{cases}, \tag{14}$$

The strain tensor components involved are given by Eqs. (9). The EEC for the interaction plane *XZ* reads as

$$\begin{aligned} p_{ef}^{(\mathrm{II})} &= \cos^2(\theta_B + \Theta)\left[p_{11}\cos^2\Theta + p_{13}\sin^2\Theta \right] + \\ &+ \sin^2(\theta_B + \Theta)\left[p_{31}\cos^2\Theta + p_{33}\sin^2\Theta \right] + 2p_{55}\sin\left(2(\theta_B + \Theta)\right)\sin\Theta\cos\Theta. \end{aligned} \tag{15}$$

The relation for $p_{ef}^{(\mathrm{II})}$ in arbitrary $X'Z$ plane of interaction is as follows:

$$\begin{aligned} p_{ef}^{(\mathrm{II})} &= \cos^2\varphi_Z \times \left\{ \cos^2(\theta_B + \Theta)(p_{11}\cos^2\Theta\cos^2\varphi_Z + p_{12}\cos^2\Theta\sin^2\varphi_Z + p_{13}\sin^2\Theta) \right. \\ &+ \sin^2(\theta_B + \Theta)(p_{31}\cos^2\Theta\cos^2\varphi_Z + p_{32}\cos^2\Theta\sin^2\varphi_Z + p_{33}\sin^2\Theta) \\ &\left. + 2p_{55}\sin\left(2(\theta_B + \Theta)\right)\sin\Theta\cos\Theta) \right\} \\ &+ \sin^2\varphi_Z \left\{ \cos^2(\theta_B + \Theta)\left[p_{21}\cos^2\Theta\cos^2\varphi_Z + p_{22}\cos^2\Theta\sin^2\varphi_Z + p_{23}\sin^2\Theta \right] \right. \\ &+ \sin^2(\theta_B + \Theta)\left[p_{31}\cos^2\Theta\cos^2\varphi_Z + p_{32}\cos^2\Theta\sin^2\varphi_Z + p_{33}\sin^2\Theta \right] \\ &\left. + 2p_{55}\sin\left(2(\theta_B + \Theta)\right)\sin\Theta\cos\Theta \right\} \end{aligned} \tag{16}$$

Similarly, the $p_{ef}^{(\mathrm{II})}$ parameter for arbitrary XZ' plane of interaction may be represented as

$$\begin{aligned} p_{ef}^{(\mathrm{II})} &= (1 - \cos^2\varphi_X \cos^2(\Theta + \theta_b)) \\ &\times (p_{31}\cos^2\Theta + p_{32}\sin^2\Theta\sin^2\varphi_X + p_{33}\sin^2\Theta\cos^2\varphi_X) \\ &+ \cos^2\varphi_X \cos^2(\Theta + \theta_b) \\ &\times (p_{11}\cos^2\Theta + p_{12}\sin^2\Theta\sin^2\varphi_X + p_{13}\sin^2\Theta\cos^2\varphi_X) + \\ &+ p_{55}\sqrt{(1 - \cos^2\varphi_X\cos^2(\Theta + \theta_b))\cos^2(\Theta + \theta_b)}\cos^2\varphi_X \sin 2\Theta \end{aligned} \tag{17}$$

The peculiarity of this AO interaction type is that the AOFM almost does not depend on the angle of rotation of the interaction plane around the *Z* axis.

Finally, the AOFM for the type (II) of AO interaction is given by the relation

$$M_2^{(\mathrm{II})} = \frac{n^6 \left\{ p_{ef}^{(\mathrm{II})} \right\}^2}{\rho \left[v_{QL}(\Theta, \varphi_{Z,X}) \right]^3}, \tag{18}$$

As seen from Fig. 6 and Fig. 7, this AO interaction type is characterized by higher AOFM value. Its value found for the XZ' plane is about $M_2^{(\mathrm{II})} = 69.4 \times 10^{-15}\ \mathrm{s^3/kg}$ at Θ =111, 291 deg and $\varphi_X = 0$ and 180 deg (see Fig. 7). The anisotropy of AOFM is mainly influenced by the anisotropy of EEC.

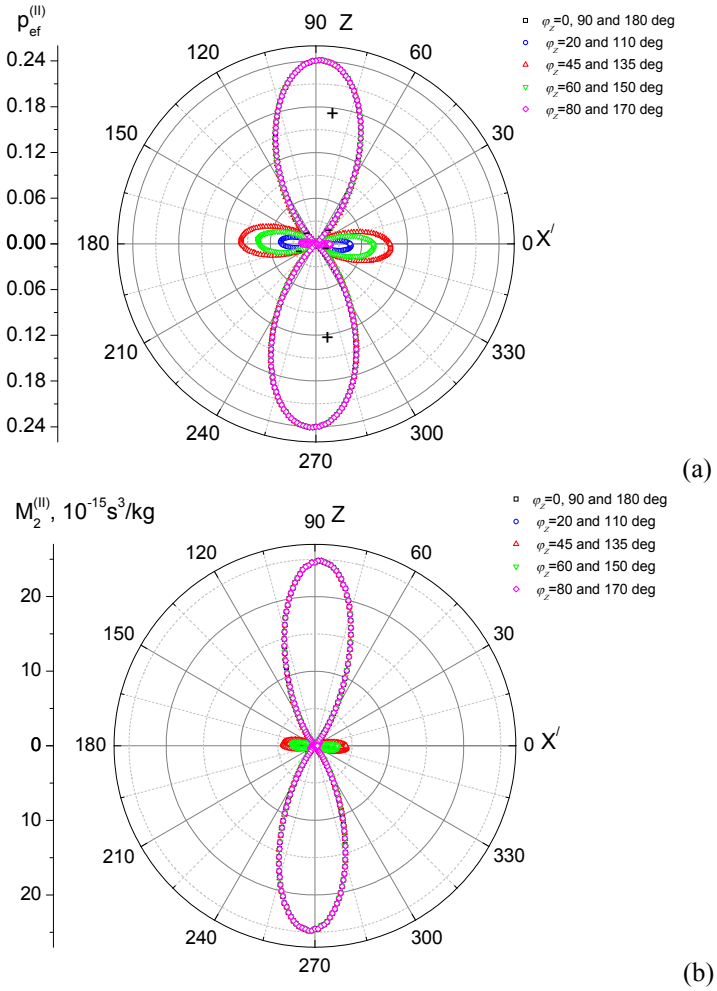

Fig. 6. Dependences of EEC (a) and AOFM $M_2^{(\mathrm{II})}$ (b) on the direction of AW vector at different orientations of the interaction plane (φ_Z is angle of rotation around the *Z* axis).

Now let us consider the type (III) of AO interaction of the optical wave, whose polarization vector lies in the *XZ* plane at the angle θ_B with respect to the *X* axis, with the transverse AW $v_{13} = v_{QT_1}$ propagating along the *X* axis and polarized along the *Z* axis. Here we have $D_3 = D\sin\theta_B$ and $D_1 = D\cos\theta_B$, and the strain tensor caused by the AW contains a single component e_5. When the AW vector direction changes in the *XZ* plane by the angle Θ, the following components of the strain tensor appear:

$$e'_1 = e_5 \sin 2\Theta,\ e'_3 = -e_5 \sin 2\Theta,\ e'_5 = e_5 \cos 2\Theta\,. \tag{19}$$

The dependence of the EEC on the AW vector direction in the *XZ* plane is given by

$$\begin{aligned} p_{ef}^{(\mathrm{III})} &= \cos^2\left(\theta_B + \Theta\right)\left[p_{11} - p_{13}\right]\sin\Theta\cos\Theta \\ &+ \sin^2\left(\theta_B + \Theta\right)\left(p_{31} - p_{33}\right)\sin\Theta\cos\Theta \\ &+ p_{55}\sin\left(2\left(\theta_B + \Theta\right)\right)\left(\cos^2\Theta - \sin^2\Theta\right) \end{aligned} \tag{20}$$

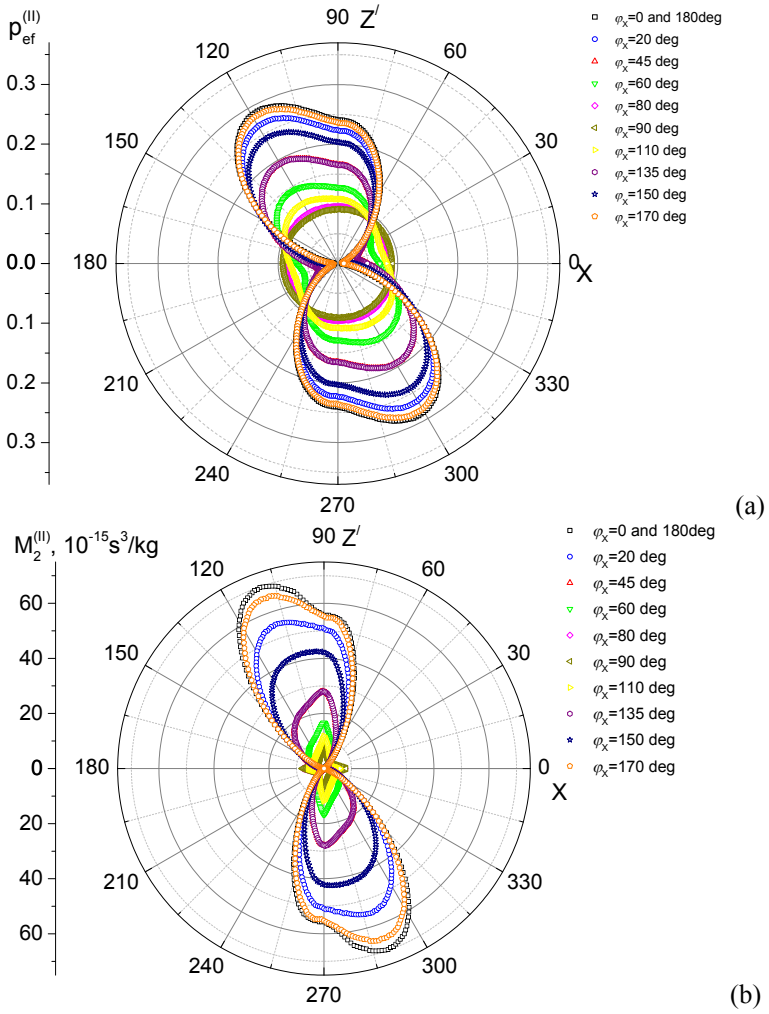

Fig. 7. Dependences of EEC (a) and AOFM $M_2^{(II)}$ (b) on the direction of AW vector (angle Θ) at different orientations of the interaction plane (φ_X is angle of rotation around the *X* axis).

For arbitrary $X'Z$ and XZ' planes, the components of deformation tensor are as follows: $e''_1 = e'_1 \cos^2 \varphi_Z$, $e''_2 = e'_1 \sin^2 \varphi_Z$, $e''_3 = e'_3$, $e''_4 = -e'_5 \sin \varphi_Z$, $e''_5 = e'_5 \cos \varphi_Z$, $e''_6 = -0.5 e'_1 \sin \varphi_Z \cos \varphi_Z$ and $e'''_1 = e'_1$, $e'''_2 = e'_3 \sin^2 \varphi_X$, $e'''_3 = e'_3 \cos^2 \varphi_X$, $e'''_4 = -0.5 e'_3 \sin \varphi_X \cos \varphi_X$, $e'''_5 = e'_5 \cos \varphi_X$, $e'''_6 = -e'_5 \sin \varphi_X$. The relation (20) should be generalized to

$$\begin{aligned} p_{ef}^{(III)} &= \cos^2 \varphi_Z [\cos^2 (\theta_B + \Theta)(p_{11} \cos^2 \varphi_Z + p_{12} \sin^2 \varphi_Z - p_{13}) \sin \Theta \cos \Theta + \\ &+ \sin^2 (\theta_B + \Theta)(p_{31} \cos^2 \varphi_Z + p_{32} \sin^2 \varphi_Z - p_{33}) \sin \Theta \cos \Theta \\ &+ p_{55} \sin (2(\theta_B + \Theta))(\cos^2 \Theta - \sin^2 \Theta))] \\ &+ \sin^2 \varphi_Z [\cos^2 (\theta_B + \Theta)\left[p_{21} \cos^2 \varphi_Z + p_{22} \sin^2 \varphi_Z - p_{23} \right] \sin \Theta \cos \Theta + \\ &+ \sin^2 (\theta_B + \Theta)\left[p_{31} \cos^2 \varphi_Z + p_{32} \sin^2 \varphi_Z - p_{33} \right] \sin \Theta \cos \Theta \\ &+ p_{55} \sin (2(\theta_B + \Theta))(\cos^2 \Theta - \sin^2 \Theta)] \end{aligned} \tag{21}$$

for arbitrary $X'Z$ plane, whereas for arbitrary XZ' plane, Eq. (20) is replaced by

$$\begin{aligned} p_{ef}^{(\mathrm{III})} &= (1-\cos^2\varphi_X\cos^2(\Theta+\theta_b))(p_{31}+p_{32}\sin^2\varphi_X-p_{33}\cos^2\varphi_X)\sin\Theta\cos\Theta \\ &+\cos^2\varphi_X\cos^2(\Theta+\theta_b)(p_{11}+p_{12}\sin^2\varphi_X-p_{13}\cos^2\varphi_X)\sin\Theta\cos\Theta+ \\ &+p_{55}\sqrt{(1-\cos^2\varphi_X\cos^2(\Theta+\theta_b))\cos(\Theta+\theta_b)^2}\cos\varphi^2{}_X(\cos^2\Theta-\sin^2\Theta) \end{aligned} . \quad (22)$$

Then the AOFM reads as

$$M_2^{(\mathrm{III})} = \frac{n^6\left\{p_{ef}^{(\mathrm{III})}\right\}^2}{\rho\left[v_{QT_1}(\Theta,\varphi_{Z,X})\right]^3}. \quad (23)$$

As seen from Fig. 8, 9 the EEC and the coefficient $M_2^{(\mathrm{III})}$ manifest petal-like dependences on the AW vector direction in the $X'Z$ and XZ' planes. This type of interaction is characterized by highest AOFM values which can reach the maximum $M_2^{(\mathrm{III})}=1143.8\times10^{-15}\,\mathrm{s}^3/\mathrm{kg}$ at $\varphi_X=90$ deg and Θ=48.7, 131.3, 228.7 and 311.3 deg (see Fig. 9). The anisotropy of AOFM is a result of the anisotropy of EEC and AW slowness. However, the high value of the M_2 parameter is due to relative slowness of the AW QT_1.

The fourth type of AO interaction can be implemented in TeO_2 crystals whenever the QT_1 wave interacts with the optical wave with polarization of the ordinary beam. After rotating the AW vector by the angle Θ, the following strain tensor components arise:

$$e'_1=e_5\sin2\Theta,\ e'_3=-e_5\sin2\Theta,\ e'_5=e_5\cos2\Theta. \quad (24)$$

The corresponding change in the refractive index is then

$$\Delta n=\frac{1}{2}n_o^3(p_{21}e'_1+p_{23}e'_3). \quad (25)$$

The EEC reads as

$$p_{ef}^{(\mathrm{IV})}=(p_{12}-p_{13})\sin2\Theta. \quad (26)$$

The same relation for AO interaction in the $X'Z$ plane is given by

$$\begin{aligned} p_{ef}^{(\mathrm{IV})} &= \sin^2\varphi_Z\left(p_{11}\cos^2\varphi_Z+p_{12}\sin^2\varphi_Z-p_{13}\right)\cos\Theta\sin\Theta+ \\ &\cos^2\varphi_Z\left(p_{21}\cos^2\varphi_Z+p_{22}\sin^2\varphi_Z-p_{23}\right)\cos\Theta\sin\Theta+p_{66}\sin^2 2\varphi_Z\cos\Theta\sin\Theta \end{aligned}, \quad (27)$$

whereas for the XZ' plane we have

$$\begin{aligned} p_{ef}^{(\mathrm{IV})} &= \left[\frac{\sin\varphi_X\cot(\Theta+\theta_b)}{\sqrt{1+\sin^2\varphi_X\cot^2(\Theta+\theta_b)}}\right]^2\left(p_{11}+p_{12}\sin^2\varphi_X-p_{13}\cos^2\varphi_X\right)\cos\Theta\sin\Theta+ \\ &+\left[\frac{1}{\sqrt{1+\sin^2\varphi_X\cot^2(\Theta+\theta_b)}}\right]^2\left(p_{21}+p_{22}\sin^2\varphi_X-p_{23}\cos^2\varphi_X\right)\cos\Theta\sin\Theta+ \\ &-p_{66}\left[\frac{2\sin\varphi_X\cot(\Theta+\theta_b)}{1+\sin^2\varphi_X\cot^2(\Theta+\theta_b)}\right]^2\sin2\varphi_X\cos\Theta\sin\Theta \end{aligned} . \quad (28)$$

As a result, the AOFM becomes as follows:

$$M_2^{(\mathrm{IV})}=\frac{n^6\left\{p_{ef}^{(\mathrm{IV})}\right\}^2}{\rho\left[v_{QT_1}(\Theta,\varphi_{Z,X})\right]^3}. \quad (29)$$

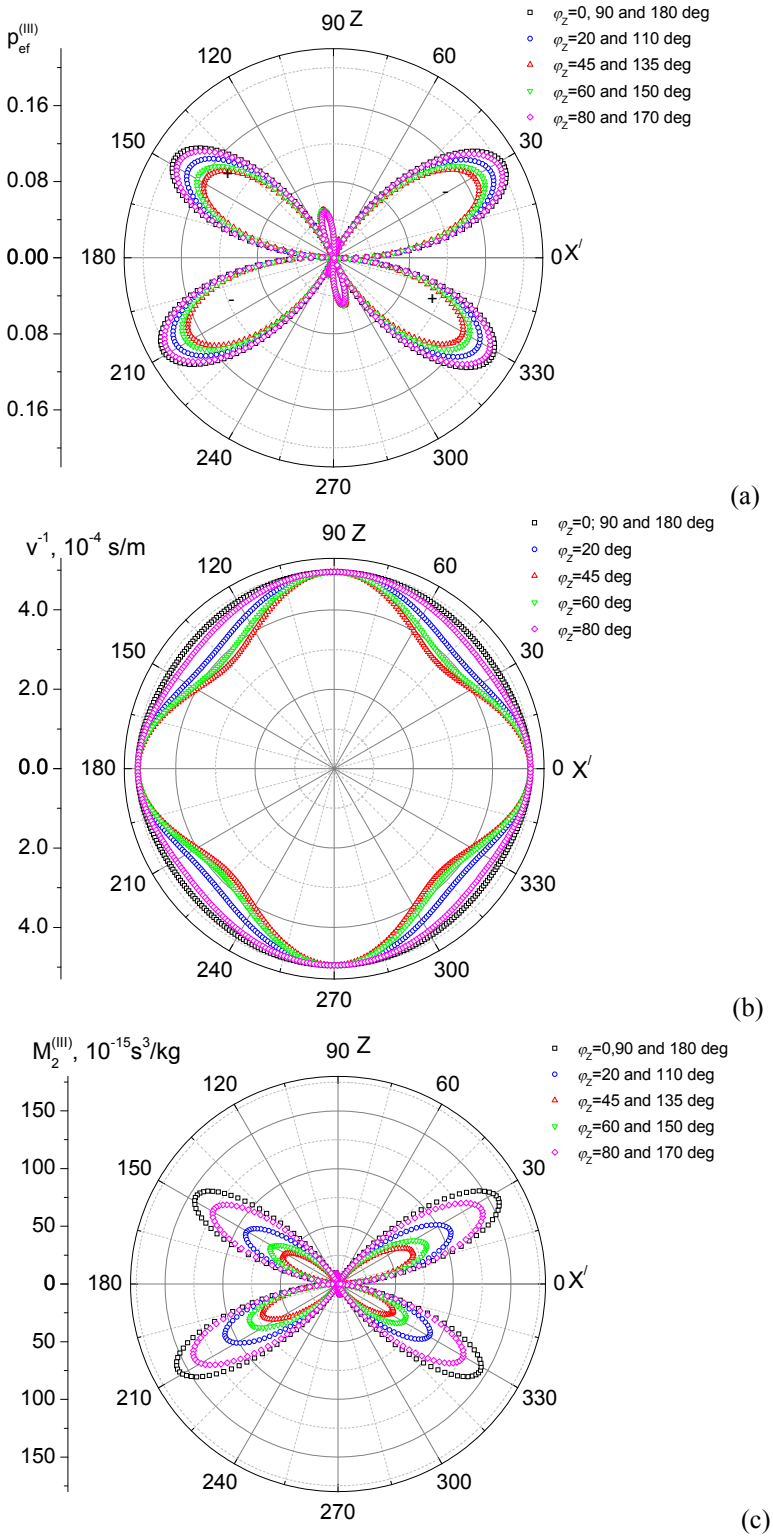

Fig. 8. Dependences of EEC (a), AW slowness (b) and AOFM $M_2^{(III)}$ (c) on the angle Θ for different orientations of AO interaction plane (φ_Z is angle of rotation around the *Z* axis).

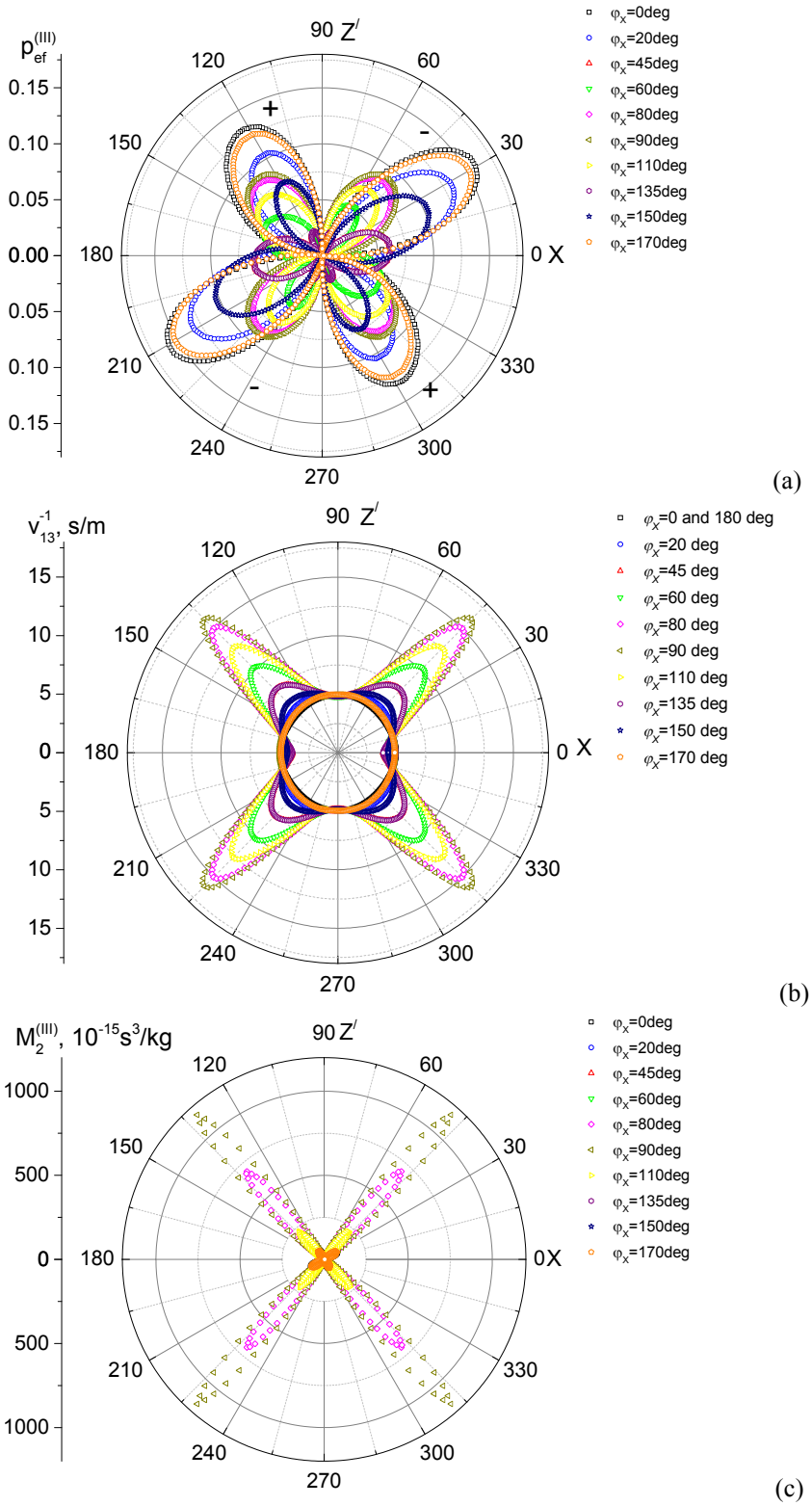

Fig. 9. Dependences of EEC (a), AW slowness (b) and AOFM $M_2^{(III)}$ (c) on the angle Θ for different orientations of AO interaction plane (φ_X is angle of rotation around the *X* axis).

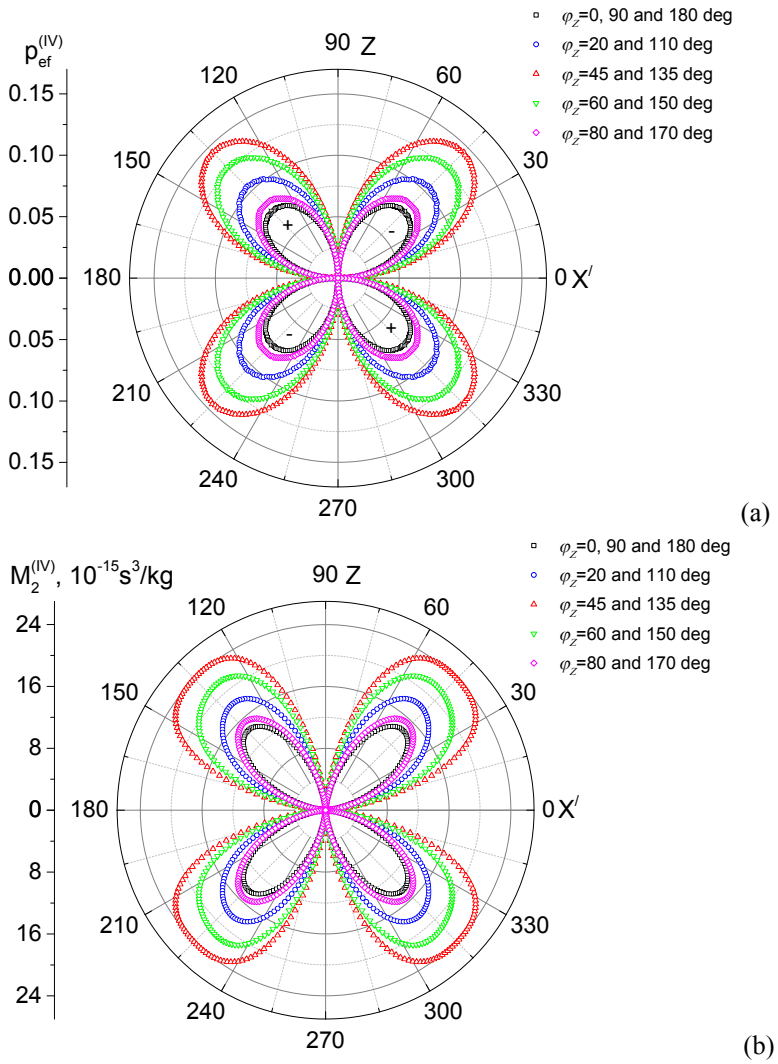

Fig. 10. Dependences of EEC (a) and AOFM $M_2^{(\mathrm{IV})}$ (b) on the angle Θ for different orientations of AO interaction plane (φ_Z is angle of rotation around the *Z* axis).

Similarly to the previous cases, the EEC and the coefficient $M_2^{(\mathrm{IV})}$ show petal-like dependences on the AW vector direction in the *XZ* plane (see Fig. 10 and Fig. 11). Notice that the EEC surface contains sections that differ by their signs. The AOFM reaches its maximum $M_2^{(\mathrm{IV})} = 892.5\times10^{-15}\,\mathrm{s}^3/\mathrm{kg}$ at $\varphi_X = 90\,\mathrm{deg}$ and Θ=44, 136, 224 and 316 deg (see Fig. 11b). The anisotropy of AOFM is caused by the both anisotropies of EEC and AW velocities.

Let us analyze the AO interaction of optical waves with the AW QT_2 ($v_{12} = v_{QT_2}$) propagating along the *X* axis and polarized along the *Y* axis, which produces the strain tensor component e_6. Depending on the orientation of electric induction of the incident light wave (i.e., availability of the components D_2, $D_3 = D\sin\theta_B$ and $D_1 = D\cos\theta_B$ whenever the interaction plane is *XZ* plane), the AO interactions of the types (V) or (VI) are dealt with. Regarding the type (V), the strain tensor includes the two components dependent upon the AW vector orientation:

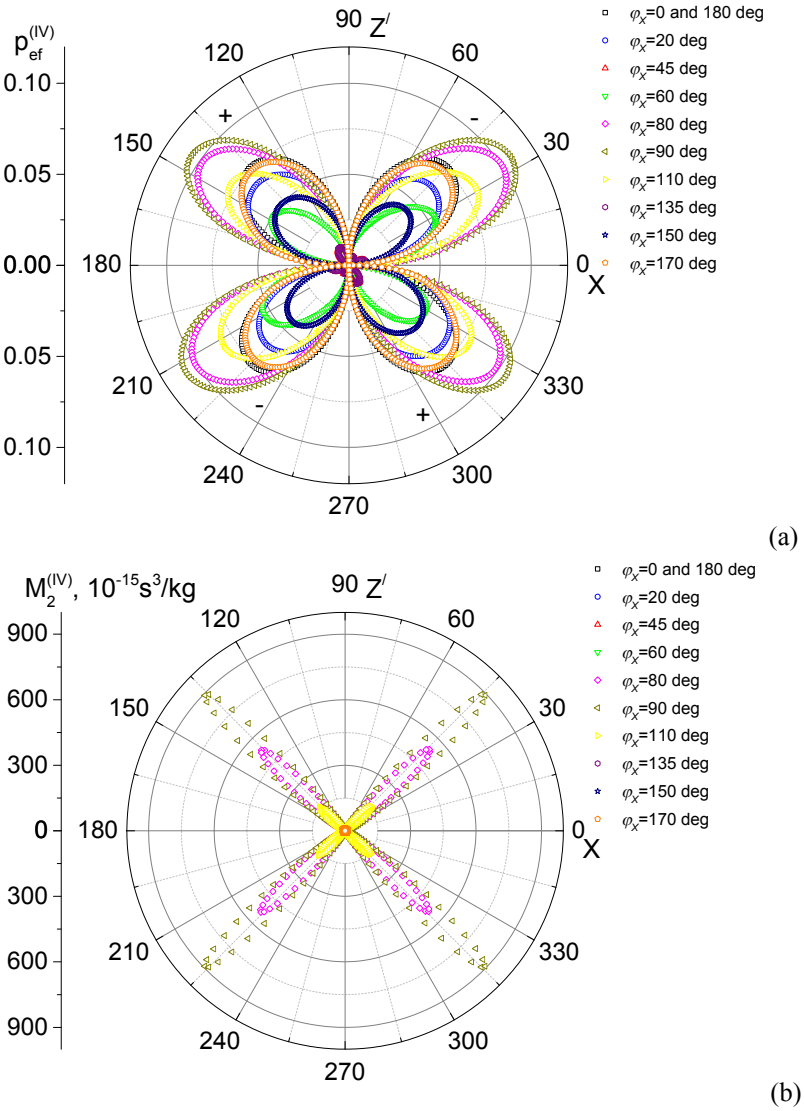

Fig. 11. Dependences of EEC (a) and AOFM $M_2^{(IV)}$ (b) on the angle Θ for different orientations of AO interaction plane (φ_X is angle of rotation around the *X* axis).

$$e'_6 = 2e_{12}\cos\Theta, \quad e'_4 = -2e_{12}\sin\Theta. \tag{30}$$

Then the increment of the optical-frequency impermeability tensor and the corresponding increment of the refractive index reduce respectively to

$$\Delta B_2 = p_{26}e_6\cos\Theta = 0 \tag{31}$$

and

$$p_{ef}^{(V)} = p_{26}\cos\Theta = 0. \tag{32}$$

At the rotation of the interaction plane around the *Z* axis the components of deformation tensor are $e''_1 = e'_6\sin\varphi_Z\cos\varphi_Z$, $e''_2 = -e'_6\sin\varphi_Z\cos\varphi_Z$, $e''_3 = 0$, $e''_4 = e'_4\cos\varphi_Z$, $e''_5 = e'_4\sin\varphi_Z$ that lead to:

$$\Delta B''_2 = 0.5\sin^2\varphi_Z\left(p_{11}-p_{12}\right)\cos\Theta\sin 2\varphi_Z$$
$$+0.5\cos^2\varphi_Z\left(p_{11}-p_{12}\right)\cos\Theta\sin 2\varphi \ , \qquad (33)$$
$$+p_{66}\sin 2\varphi_Z\cos\Theta\cos 2\varphi_Z$$

$$\Delta n = -\frac{1}{2}n_e^3(0.5\sin^2\varphi_Z\left(p_{11}-p_{12}\right)\cos\Theta\sin 2\varphi_Z$$
$$+0.5\cos^2\varphi_Z\left(p_{11}-p_{12}\right)\cos\Theta\sin 2\varphi \qquad , \qquad (34)$$
$$+p_{66}\sin 2\varphi_Z\cos\Theta\cos 2\varphi_Z)$$

with the EEC being equal to

$$p_{ef}^{(\mathrm{V})} = 0.5\sin^2\varphi_Z\left(p_{11}-p_{12}\right)\cos\Theta\sin 2\varphi_Z$$
$$+0.5\cos^2\varphi_Z\left(p_{11}-p_{12}\right)\cos\Theta\sin 2\varphi_Z \cdot$$
$$+0.5p_{66}\sin 2\varphi_Z\cos\Theta\cos 2\varphi_Z$$

Finally, rotation of the interaction plane around the X axis results in deformation tensor components $e'''_2 = -e'_4\sin\varphi_X\cos\varphi_X$, $e'''_3 = e'_4\sin\varphi_X\cos\varphi_X$, $e'''_1 = 0$, $e'''_4 = e'_4\cos 2\varphi_X$, $e'''_5 = e'_6\sin\varphi_X$, $e'''_6 = e'_6\cos\varphi_X$. Then the EEC is given by relation:

$$p_{ef}^{(\mathrm{V})} = \left[\frac{\sin\varphi_X\cot(\Theta+\theta_b)}{\sqrt{1+\sin^2\varphi_X\cot^2(\Theta+\theta_b)}}\right]^2\left(p_{12}-p_{13}\right)\sin\Theta\sin\varphi_X\cos\varphi_X$$

$$+\left[\frac{1}{\sqrt{1+\sin^2\varphi_X\cot^2(\Theta+\theta_b)}}\right]^2\left(p_{22}-p_{23}\right)\sin\Theta\sin\varphi_X\cos\varphi_X \ , \qquad (35)$$

$$+0.5p_{66}\left[\frac{2\sin\varphi_X\cot(\Theta+\theta_b)}{1+\sin^2\varphi_X\cot^2(\Theta+\theta_b)}\right]\cos\Theta\cos\varphi_X$$

Then the AOFM is as follows:

$$M_2^{(\mathrm{V})} = \frac{n^6\left\{p_{ef}^{(\mathrm{V})}\right\}^2}{\rho\left[v_{QT_2}(\Theta,\varphi_{Z,X})\right]^3} \ . \qquad (36)$$

The AOFM becomes the highest for the direction where the AW is the slowest ($M_2^{(\mathrm{V})} = 753.3\times10^{-15}\,\mathrm{s}^3/\mathrm{kg}$ at $\varphi_Z = 45$ or 135 deg and $\Theta = 0$ or 180 deg). The dependences of the $M_2^{(\mathrm{V})}$ coefficient on the angles φ_Z and Θ are depicted in Fig. 12. As seen from Fig. 12, the dependence of AOFM in the $X'Z$ plane on the angle Θ is similar to that of the $p_{ef}^{(\mathrm{V})}$ parameter. Notice that $p_{ef}^{(\mathrm{V})}$ is equal to zero at $\varphi_Z = 90$, and 270 deg, when the AO diffraction does not occur at all. It is also interesting that the EEC surface consists of sections with the opposite signs.

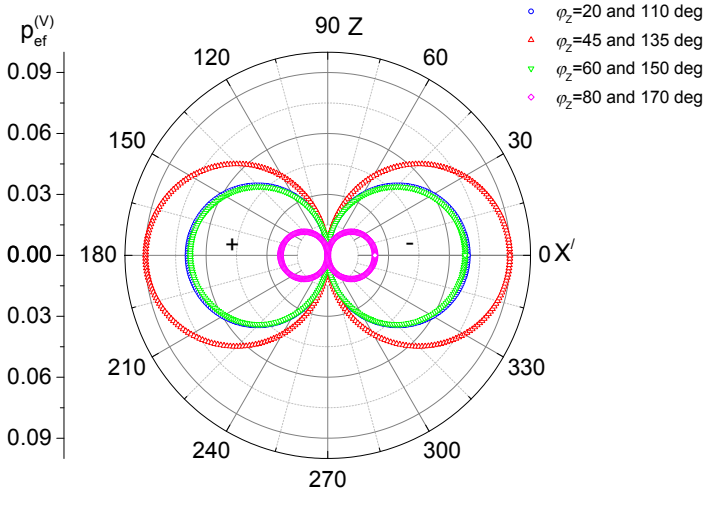

(a)

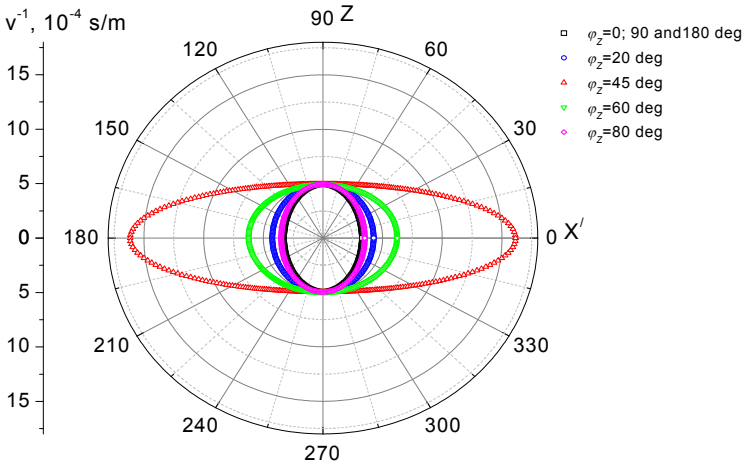

(b)

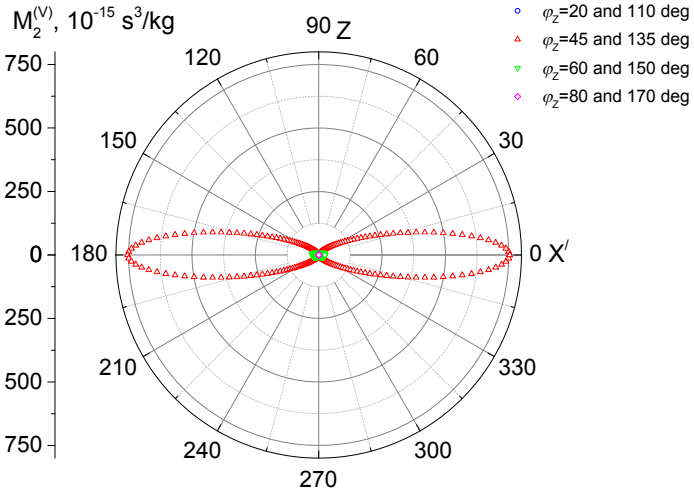

(c)

Fig. 12. Dependences of EEC (a) AW slowness (b) and AOFM $M_2^{(V)}$ on the angle Θ for different orientations of AO interaction plane (φ_Z is angle of rotation around the *Z* axis).

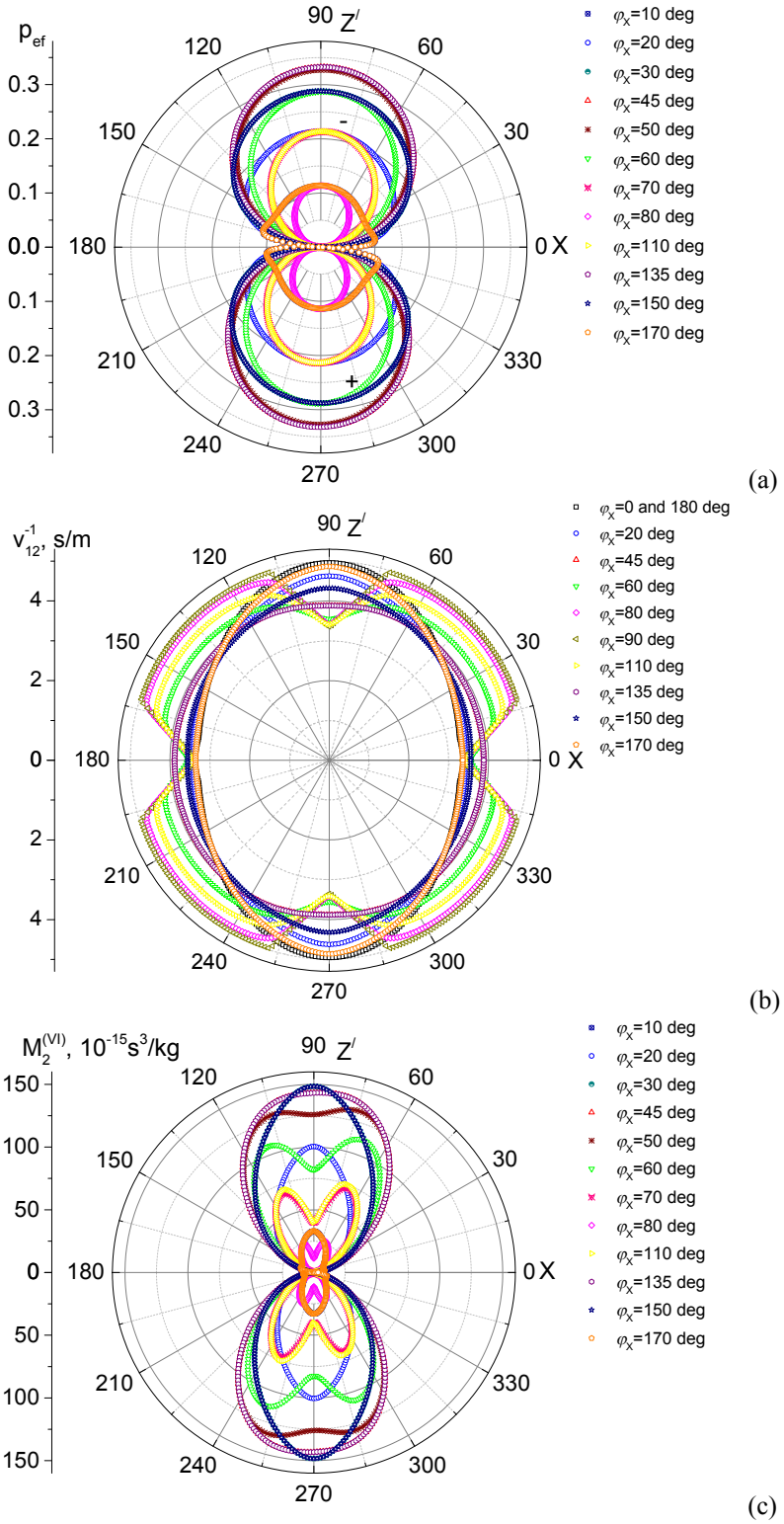

Fig. 13. Dependences of EEC (a) AW slowness (b) and AOFM $M_2^{(V)}$ (c) on the angle Θ for different orientations of AO interaction plane (φ_X is angle of rotation around the *X* axis).

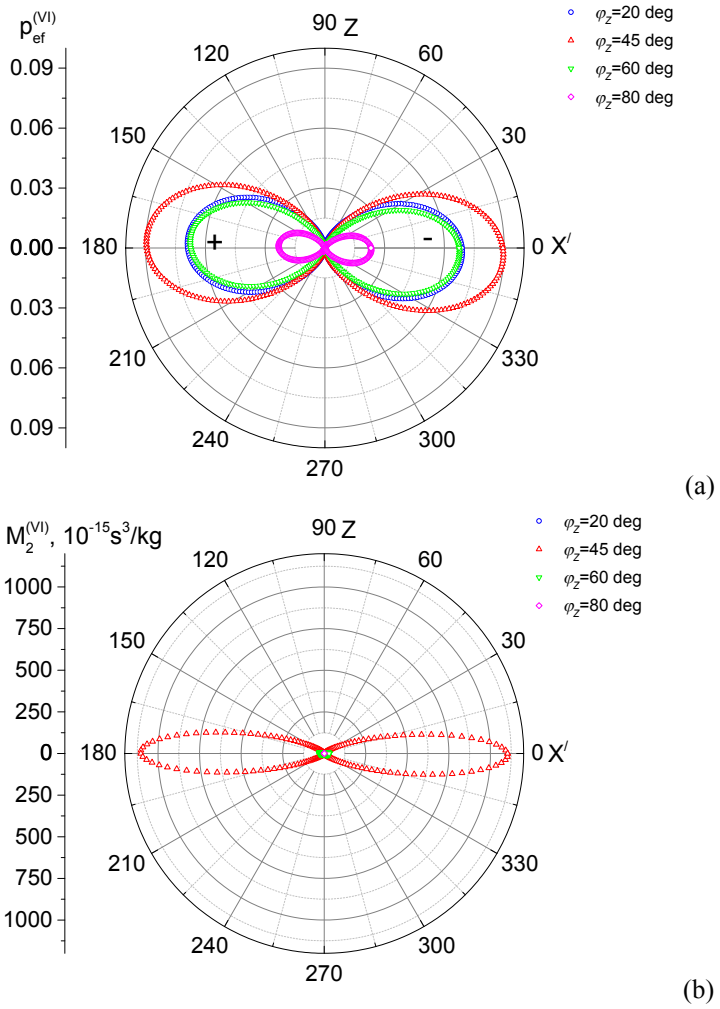

Fig. 14. Dependences of EEC (a) and AOFM $M_2^{(VI)}$ (b) on the angle Θ for different orientations of AO interaction plane (φ_Z is angle of rotation around the *Z* axis).

Our final step is to consider the type (VI) of AO interaction when the polarizations of the incident and diffracted optical waves belong to the $X'Z$ plane. According to Eqs. (30), the increment of the refractive index induced by the strains appearing due to the AW, and the EEC are given by

$$\Delta n = -\frac{1}{2} n_e^3 (\cos^2(\theta_B + \Theta) p_{16}) e_6 \cos\Theta = 0\,, \tag{37}$$

$$p_{ef}^{(VI)} = (\cos^2(\theta_B + \Theta) p_{16}) \cos\Theta = 0\,, \tag{38}$$

The dependence of EEC on the angle φ_Z is as follows:

$$\begin{aligned} p_{ef}^{(VI)} &= \cos^2\varphi_Z [\cos^2(\theta_B + \Theta)(p_{11} - p_{12}) \cos\Theta \cos\varphi_Z \sin\varphi_Z] \\ &+ \sin^2\varphi_Z [\cos^2(\theta_B + \Theta)(p_{11} - p_{12}) \cos\Theta \cos\varphi_Z \sin\varphi_Z]\,. \\ &+ 0.5 p_{66} \sin 2\varphi_Z \cos\Theta \cos 2\varphi_Z \end{aligned} \tag{39}$$

Rotation of the interaction plane around the *X* axis results in

$$p_{ef}^{(\mathrm{VI})} = (1-\cos^2\varphi_X\cos^2(\Theta+\theta_b))(p_{32}-p_{33})\sin\Theta\sin\varphi_X\cos\varphi_X + \cos^2\varphi_X\cos^2(\Theta+\theta_b)(p_{12}-p_{13})\sin\Theta\sin\varphi_X\cos\varphi_X, \quad (40)$$

$$M_2^{(\mathrm{VI})} = \frac{n^6\left\{p_{ef}^{(\mathrm{VI})}\right\}^2}{\rho\left[v_{QT_2}(\Theta,\varphi_{Z,X})\right]^3}. \quad (41)$$

As seen from Fig. 14 and Fig. 15, the AOFM $M_2^{(\mathrm{VI})}$ reaches its maximal equal to $1102.9\times10^{-15}\,\mathrm{s}^3/\mathrm{kg}$ at $\Theta = 0$ or 180 deg and $\varphi_Z = 45$ deg.

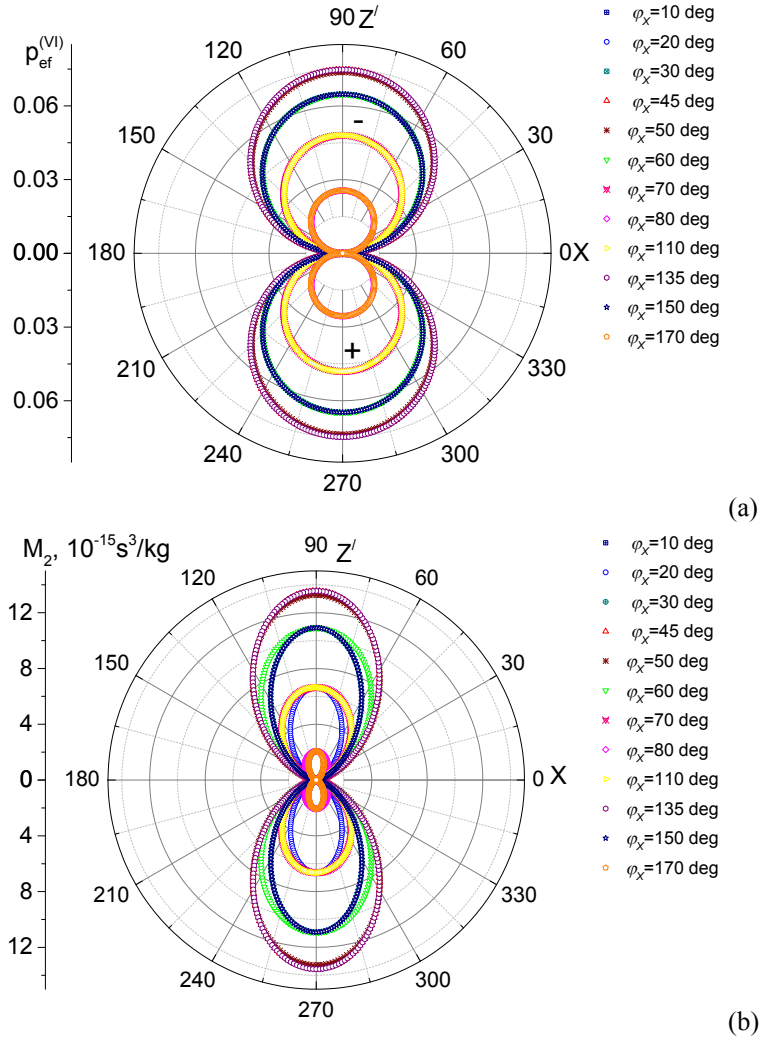

Fig. 15. Dependences of EEC (a) and AOFM $M_2^{(\mathrm{VI})}$ (b) on the angle Θ for different orientations of AO interaction plane (φ_X is angle of rotation around the *X* axis).

3. Conclusions

Table 1 represents the AOFM values calculated for different geometries of isotropic AO interactions in TeO_2 crystals, using the technique described above. One can notice good agreement

of the calculated values and the experimental data reported in Ref. [10]. Some small differences among those results may be caused by the fact that our calculations do not account for non-orthogonality (or non-longitudity) of polarizations of the AWs, as well as the influence of piezoelectric effect on the AW velocities. Nonetheless, we conclude that the method developed in the present work is applicable for calculating the anisotropy of AOFM in optically uniaxial crystalline materials. Table 2 summarizes the maximal AOFM values typical for the six different types of isotropic AO interactions possible in TeO_2.

Table 1. Conditions of isotropic AO interactions and experimental AO parameters of TeO_2 crystals reported in Ref. [10], together with the corresponding parameters calculated in this work.

AW		v, m/s [10]	Optical wave		EEC p_{ef}[10]	Experimental AOFM, 10^{-15} s^3/kg [10]	Calculated AOFM, 10^{-15} s^3/kg
Propagation direction	Polarization direction		Propagation direction	Polarization direction			
[100]	[100]	2980	[010]	[100]	p_{11}	0.048	0.044
[100]	[100]	2980	[010]	[001]	p_{31}	10.6	8.0
[001]	[001]	4260	[010]	[100]	p_{13}	34.5	33.3
[001]	[001]	4260	[010]	[001]	p_{33}	25.6	24.7
[110]	[110]	4210	$[\bar{1}10]$	[110]	$(p_{11}+p_{12}+2p_{66})/2$	0.802	0.772
[110]	[110]	4210	[110]	[001]	p_{31}	3.77	3.00
[101]	[101]	3640	$[\bar{1}01]$	[010]	$(p_{12}+p_{13})/2$	33.4	32.1
[110]	$[1\bar{1}0]$	617	[001]	arbitrary	$(p_{11}-p_{12})/2$	793	928*
[101]	$[10\bar{1}]$	2080	[010]	[100]	$(p_{11}-p_{13})/2$	77.7	55.0

*M_2 is calculated as the mean value of AOFM's which are equal to 1102.9×10^{-15} s^3/kg and 753.3×10^{-15} s^3/kg .

Table 2. Maximal values of AOFM M_2 calculated for different types of AO interactions in TeO_2 crystals and description of the corresponding geometries.

Type of AO interaction	Propagation direction of AW		Type of AW	Polarization of incident optical wave	AOFM M_2, 10^{-15} s^3/kg
	Angle Θ, deg	Angle $\varphi_{Z,X}$, deg			
(I)	90	$\varphi_Z = 0$ and 180	QL	parallel to [010] direction	33.8
(II)	111, 291	φ_X =0 and 180	QL	almost parallel to the direction of propagation of the AW	69.4
(III)	48.7, 131.3, 228.7 and 311.3	φ_X =90	QT_1	almost parallel to [001] direction	1143.8
(IV)	44, 136, 224 and 316	φ_X =90	QT_1	almost parallel to [110] direction	892.5
(V)	0 and 180	φ_Z =45 and 135	QT_2	parallel to [110] direction	753.3
(VI)	0 and 180	φ_Z =45	QT_2	almost parallel to [110] direction	1102.9

As seen from Table 2, the maximal AOFM characteristic for the AO interaction with the quasi-longitudinal wave is not high enough, being equal to $69.4\times10^{-15}\,\mathrm{s}^3/\mathrm{kg}$. This value corresponds to the type (II) of AO interactions. Higher M_2 values are typical for the types (III), (IV), (V) and (VI) of AO interactions with the QT_1 and QT_2 waves. Following from our AO anisotropy analysis performed for all of the cases of isotropic diffractions in TeO_2 crystals, we conclude that the highest M_2 value ($M_2^{(\mathrm{III})}=1143.8\times10^{-15}\,\mathrm{s}^3/\mathrm{kg}$) is reached when we deal with the type (III) of AO interaction. Then the incident optical wave polarized almost parallel to [001] direction and propagating in the *XY* plane (i.e., in the crystallographic plane *ab*) interacts with the quasi-transverse AW QT_1 propagating in the *ab* plane almost parallel to [110] direction and polarized parallel to $[\bar{1}10]$ direction. This high M_2 value represents a combined consequence of both high EEC value and a slowness of the AW.

References

1. Shaskolskaya M P, Acoustic crystals. Moscow: Nauka, 1982.
2. Uchida N, 1971. Optical properties of single-crystals paratellurite (TeO_2). Phys. Rev. B. **4**: 3736–3745.
3. Singh N B and Duval W M B 1991. Growth kinetics of physical vapour transport processes: Crystal growth of opto-electronic material mercurous chloride. NASA Technical Memorandum. 103788.
4. Singh B, Hopkins R H, Suhre D R, Taylor L H, Rosch W, Gottlieb M, Duval W M B, Glicksman M E and Northrop Grumman, 1999. Physical vapor transport growth of mercuroushalide crystals for acousto-optic tunable filters. Technical Program. The 128th TMS Annual Meeting & Exhibition. San Diego, California, U.S.A. February 28 – March 4, 36.
5. Gottlieb M, Isaacs T J, Feichtner J D and Roland G W, 1974. Acousto-optic properties of some chalcogenide crystals. J. Appl. Phys. **45**: 5145–5151.
6. Vlokh R and Martynyuk-Lototska I 2009. Ferroelastic crystals as effective acoustooptic materals. Ukr. J. Phys. Opt. **10**: 89–99.
7. Peercy P S and Fritz I J, 1974. Pressure-induced phase transition in paratellurite (TeO_2). Phys. Rev. Lett. **32**: 466–469.
8. McWhan D B, Birgeneau R J, Bonner W A, Taub H and Ace J D, 1975. Neutron scattering study at high pressure of the structural phase transition in paratellurite. J. Phys. C: Solid State Phys. **8**: L81–L85.
9. Yanj T and Watanabe A, 1974. Acousto-optic figure of merit of TeO_2 for circularly polarized light. J. Appl. Phys. **45**: 1243–1245.
10. N. Uchida and Y. Ohmachi 1969. Elastic and photoelastic properties of TeO_2 single crystal. J. Appl. Phys. **40**: 4692–4695.
11. Mys O, Kostyrko V, Smyk M, Krupych O and Vlokh R, 2014. Anisotropy of acoustooptic figure of merit in optically isotropic media. Appl. Opt. **53** (to be published); arXiv:1405.1919 [phyics.optics].

Mys O., Kostyrko M., Smyk M., Krupych O. and Vlokh R. 2014. Anisotropy of acoustooptic figure of merit for TeO_2 crystals. 1. Isotropic diffraction Ukr.J.Phys.Opt. **15**: 132–154.

Анотація. *Запропоновано метод аналізу анізотропії коефіцієнта акустооптичної якості для оптично одновісних кристалів на прикладі кристалічного парателуриту. В першій частині статті представлено результати аналізу ізотропної акустоптичної взаємодії. Дані розрахунків добре узгоджуються з відомими експериментальними результатами.*